

Exploring a Non-ATP Pocket for Potential Allosteric Modulation of PI3K α

Paraskevi Gkekka,[†] Alexandra Papafotika,^{‡,§} Savvas Christoforidis,^{‡,§} and Zoe Cournia*,[†]

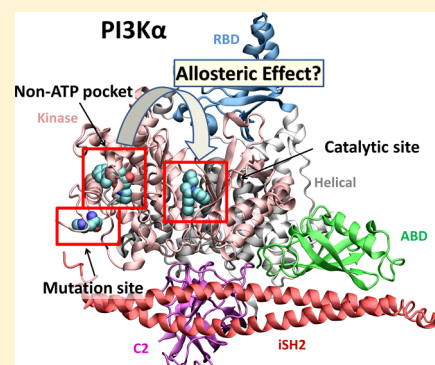
[†]Biomedical Research Foundation, Academy of Athens, 4 Soranou Ephessiou, 11527 Athens, Greece

[‡]Institute of Molecular Biology and Biotechnology-Department of Biomedical Research, Foundation for Research and Technology (IMBB-BR/FORTH), 45110 Ioannina, Greece

[§]Laboratory of Biological Chemistry, Department of Medicine, University of Ioannina, 45110 Ioannina, Greece

Supporting Information

ABSTRACT: Allosteric modulators offer a novel approach for kinase inhibition because they target less conserved binding sites compared to the active site; thus, higher selectivity may be obtained. PIK-108, a known pan phosphoinositide 3-kinase (PI3K) inhibitor, was recently detected to occupy a non-ATP binding site in the PI3K α C-lobe. This newly identified pocket is located close to residue 1047, which is frequently mutated in human cancers (H1047R). In order to assess the interactions, stability, and any possible allosteric effects of this inhibitor on PI3K α , extensive molecular dynamics (MD) simulations in aqueous solution were performed for the wild type (WT) human, WT murine, and H1047R human mutant PI3K α proteins with PIK-108 placed in both catalytic and non-ATP sites. We verify the existence of the second binding site in the vicinity of the hotspot H1047R PI3K α mutation through binding site identification and MD simulations. PIK-108 remains stable in both sites in all three variants throughout the course of the simulations. We demonstrate that the pose and interactions of PIK-108 in the catalytic site are similar in the murine WT and human mutant forms, while they are significantly different in the case of human WT PI3K α protein. PIK-108 binding in the non-ATP pocket also differs significantly among the three variants. Finally, we examine whether the non-ATP binding site is implicated in PI3K α allostery in terms of its communication with the active site using principal component analysis and perform *in vitro* experiments to verify our hypotheses.



1. INTRODUCTION

Protein kinases are enzymes crucial for a multitude of fundamental biological processes and coordination of complex functions such as regulation of the cell cycle and signal transduction. Phosphoinositide 3-kinases (PI3Ks) are a family of intracellular signal transducer enzymes that catalyze the phosphorylation of the 3-position hydroxyl group of the inositol ring of phosphatidylinositols. They are divided into three classes: class I, II, and III. Class I PI3Ks are further classified into four isoforms: PI3K α , PI3K β , PI3K γ , and PI3K δ .¹ These isoforms are characterized by distinct substrate specificities and have discrete roles in cellular processes, being involved in cell survival, proliferation, differentiation, and metabolism. PI3Ks have emerged as important therapeutic targets after the discovery that the PI3K pathway is frequently deregulated in a wide range of cancers;^{2–4} overactivation of these kinases leads to the reduction of apoptosis, thus allowing proliferation.^{2–5} However, a key challenge in targeting this pathway is the identification of isoform-selective inhibitors, since the four above-mentioned PI3K isoforms are involved in distinct cellular processes, including glucose homeostasis and the immune response.⁶ The high similarity of the four PI3K isoforms in the adenosine triphosphate (ATP) binding pocket often leads to the development of nonselective PI3K drug

candidates, which may yield undesirable side effects. Allosteric modulators typically bind to less conserved sites compared to the active site of an enzyme, and thus, they may confer greater specificity in kinase regulation.^{7–9}

Selective targeting of the PI3K α isoform is of particular pharmacological interest, since overactivation of PI3K α signaling is one of the most frequent events leading to cancer.^{10–12} Deregulation of the PI3K α pathway may occur by several different mechanisms, including somatic mutations and amplification of genes encoding key components of the PI3K α pathway.⁵ Somatic mutations within the PIK3CA gene, which encodes the catalytic subunit p110 α of PI3K α , are frequently observed in a variety of human tumors, including breast, colon, and endometrial cancers, as well as glioblastomas.^{10,13,14} These mutations are scattered over the length of p110 α , but two hotspots account for nearly 80% of them: an H1047R substitution in the kinase domain close to the C-terminus and a cluster of three charge-reversal mutations

Special Issue: William L. Jorgensen Festschrift

Received: June 27, 2014

Revised: October 3, 2014

Published: October 9, 2014

(E542K, E545K, Q546K) in the helical domain of p110 α .¹⁴ The importance of developing mutant-specific PI3K α inhibitors can be highlighted by the fact that PIK3CA is mutated in \sim 27% of breast cancer cases on average, in endometrial cancer in 24% of the cases, and in colon cancer in \sim 15% of the cases.¹⁵ Moreover, in a recent study, it was shown that the presence of PIK3CA mutations is associated with a poorer response in patients who receive anti-HER2 therapies;¹⁶ combination therapy with a mutant-specific PI3K α inhibitor could thus benefit PIK3CA mutant HER2-positive breast cancer patients.

PI3K α is a heterodimer; apart from the catalytic subunit, p110 α , it also contains a regulatory subunit, p85 α . The p110 α catalytic subunit comprises five domains: the adaptor-binding domain (ABD), the RAS-binding domain (RBD), and the C2, helical, and kinase domains. The p85 α subunit also consists of five domains: the Src homology 3 domain (SH3), the GTPase activating protein (GAP) domain, the N-terminal Src homology 2 domain (nSH2), the inter-SH2 domain (iSH2), and the C-terminal Src homology 2 domain (cSH2). The regulatory subunit confers stability to the catalytic subunit and diminishes its basal ATPase activity.

The crystal structures of human wild-type (WT) and H1047R PI3K α mutant have been recently solved by X-ray crystallography.^{17–19} Moreover, the structure of the murine WT PI3K α complexed with a propeller-shaped pan-PI3K inhibitor, PIK-108,⁶ was solved by Hon et al.²⁰ PIK-108 is a morpholino chromone inhibitor that is more selective for the PI3K β and PI3K δ isoforms.⁶ Hon et al. showed that, in addition to the ATP-binding pocket, a second, unexpected non-ATP binding site is observed in the kinase C-lobe, close to the H1047R mutation (Figure 1), where PIK-108 binds. This non-ATP pocket has not been observed in other PI3K α crystal structures; the human WT and human H1047R mutant have only been cocrystallized with inhibitors in their active site.^{17,21} This discovery stimulated our interest in exploring the viability of this new binding site and its potential allosteric effect on

PI3K α activity, since it is found in the vicinity of the mutation H1047R. Several studies have recently focused on unveiling the allosteric modulation of proteins with small molecules by exploiting novel binding pockets for drug discovery.^{8,9,22–29} On the basis of such approaches and the study by Hon et al., we aim to gain insights into the design of novel selective inhibitors that bind close to the mutated region of the protein.

Ligand binding underlies a wide variety of recognition processes that often remain underdescribed due to insufficient resolution of experimental techniques. The use of reliable computational methods to explore protein–ligand interactions can greatly enhance our understanding of such systems and can lead to the fast and efficient development of novel, potent protein inhibitors.^{30–32} In this study, we perform unbiased molecular dynamics (MD) simulations in aqueous solution for the WT human apo and holo forms, WT murine holo form, and human H1047R mutant apo and holo forms, with PIK-108 placed in both catalytic and non-ATP pockets. We verify the existence of this second, unexpected binding site found in the vicinity of the hotspot H1047R PI3K α mutation through binding site identification. We further demonstrate via MD simulations that PIK-108 remains stable in both the ATP and non-ATP sites in all three protein variants. We monitor the protein–ligand interactions as well as investigate the dynamics of the complexes. The PIK-108 pose and interactions in the catalytic site are almost identical in the case of murine WT and human mutant forms, while they are significantly different in the case of human WT. In all three proteins, PIK-108 interacts differently with the non-ATP pocket. We then discuss allosteric implications of the newly identified non-ATP pocket and explore connections with the catalytic site and other functionally relevant PI3K α areas of the kinase domain through principal component analysis (PCA). We demonstrate that, while the non-ATP pocket is not motionally correlated to the catalytic site, binding of PIK-108 in this pocket alters the conformation of other functionally important PI3K α elements, providing insights into the design of mutant-specific inhibitors. Finally, we perform *in vitro* assays to test whether PIK-108 acts as an allosteric inhibitor.

2. METHODS

2.1. Model Building. A detailed description of the model construction and refinement procedures is presented in the Supporting Information. In brief, atomistic models of the human and murine WT PI3K α and human H1047R mutant PI3K α were created with Modeler 9v8³³ using the respective crystal structures (PDB IDs: 2RD0, 4A55, and 3HIZ). UniProt database amino acid sequences were used to complete missing amino acid residues and protein loops with a combination of homology and loop modeling. The model of the human WT p110 α /p85 α -niSH2 was constructed using 2RD0 and 3HHM for the p110 α and p85 α (iSH2 and nSH2 domains) subunits, respectively. Distance restraints were applied to preserve important polar contacts as well as the positioning of the nSH2 domain with respect to the p110 α subunit, as found in structures 3HIZ and 3HHM of the human H1047R PI3K α . In particular, the following residue pairs were restrained to form H-bonds: 348 (p85 α) and 453 (p110 α), 380 (p85 α) and 545 (p110 α), 382 (p85 α) and 546 (p110 α), and 417 (p85 α) and 512 (p110 α). During homology and loop modeling, the p110 α subunit was kept rigid except from those residues that were in contact with p85 α -niSH2 (1–6, 357, 364–369, 410–419, 453–456, 540–549, 573, 1017, 1023,

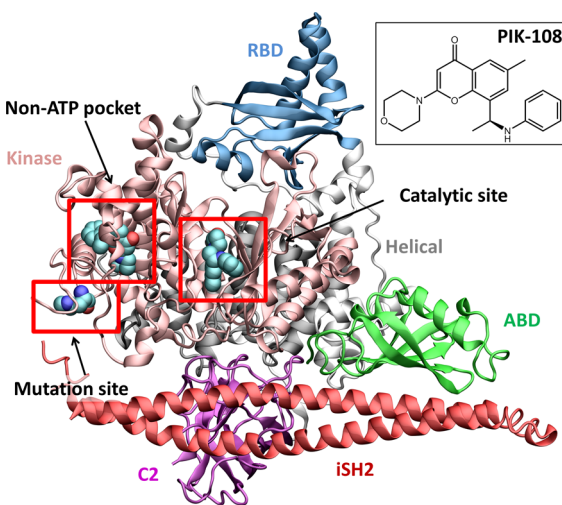


Figure 1. Crystal structure of the murine WT PI3K α ²⁰ complexed with PIK-108 in the active site and in a newly identified non-ATP pocket. PI3K α is shown in cartoon representation and is colored by domain. PIK-108 is depicted with van der Waals spheres and is colored by atom type. His1047, which is a hotspot mutation site in several types of cancer, is also shown in van der Waals spheres, colored by atom type, and is labeled as “Mutation site”. Inset: The chemical structure of PIK-108.

Table 1. List of Simulated Systems

number	system	total simulation length (ns)	simulation time used for analysis (ns)
1	murine WT (mWT)/PIK-108	140	100
2	human WT (hWT)/PIK-108	190	100
3	human H1047R mutant (hMUT)/PIK-108	260	50
4	human WT (hWT) (apo)	250	100
5	human H1047R mutant (hMUT) (apo)	150	100

1028–1029). The model of the murine WT p110 α /p85 α -niSH2 was constructed using the 4A5S and 3HHM crystal structures, in the same manner as the human homologue, using the same set of restraints. The model of the human H1047R PI3K α mutant was constructed using the 3HIZ crystal structure. Missing residues from the p85 α -niSH2 domains (322–326, 409–412, 432–446) were constructed through loop modeling, during which H1047R-p110 α residues close to p85 α -niSH2 (1–4, 342–351, 406–422, 444–453) were left flexible, whereas the rest of the H1047R-p110 α subunit was kept rigid. All the parameters used for homology and loop modeling are discussed in more detail in the Supporting Information (section A1). Simulations between proteins in the holo and apo forms started from the same configuration with the exception of the non-ATP pocket area, where slight modifications in residue positions were induced to accommodate the ligand (see below).

2.2. System Setup and MD Simulations. Five different PI3K α systems have been considered in the present study: the holo murine WT complexed with PIK-108 (mWT-holo), the human WT in the apo and holo forms complexed with PIK-108 (hWT-apo and hWT-holo), and the human H1047R variant in the apo and holo forms complexed with PIK-108 (hMUT-apo and hMUT-holo). The PIK-108 inhibitor has been cocrystallized in the mWT PI3K α in both the orthosteric and a novel non-ATP binding site²⁰ but not in the human WT or mutant counterparts. Therefore, in order to examine the possibility of PIK-108 binding at both sites of the human WT and human H1047R mutant PI3K α , we first performed binding site prediction with FTMap³⁴ in order to identify druggable cavities in these two proteins. Then, we overlapped the two structures with the crystal structure of WT murine protein using Chimera³⁵ and placed PIK-108 in the catalytic and non-ATP sites. Chimera was then used to relieve steric clashes of the ligand with the neighboring residues. Different residue rotamers were considered for clashing residues using the structure-editing tool of Chimera; rotamers with the highest probability were chosen in the final structures. For each system, we considered a rhombic dodecahedron periodic box with a minimum distance of 10 Å between the protein and the box walls to ensure that the proteins would not directly interact with their periodic image.

All simulations were performed using GROMACS 4.5.4 software³⁶ and the AMBER99SB-ILDN all-atom force field³⁷ to model the proteins and the TIP3P model for water molecules.³⁸ The force field parameters for PIK-108 were calculated using Antechamber and acpype and are based on the general Amber force field (GAFF).^{39–41} The validity of the parameters for PIK-108 was checked during a 5 ns in vacuo simulation, where the appropriate geometry of the molecule was visually inspected.

Long-range electrostatic interactions were treated using the particle-mesh Ewald summation method.⁴² The temperature during the simulations was kept constant at 310 K using a

Nosé–Hoover thermostat with a time constant of 1 ps.⁴³ The pressure was isotropically maintained at 1 atm using Parrinello–Rahman coupling with a time constant of 5 ps and compressibility of 4.5×10^{-5} bar⁻¹.⁴⁴ A time step of 2 fs was used with all bond lengths constrained using the LINCS algorithm.⁴⁵ The nonbonded potential energy functions were switched, with forces smoothly decaying between 8 and 10 Å for the van der Waals and from 0 to 11 Å for the short-range electrostatic interactions. Prior to MD simulations, all the structures were relaxed by 10 000 steps of energy minimization using the steepest descent algorithm, followed by position restraint equilibration first in the NVT and then in the NPT ensemble for 200 ps, respectively. Finally, unbiased MD simulations were carried out (see Table 1 for details).

2.3. Convergence and Analysis Protocols. To ensure convergence of the simulated systems, we first calculated the backbone α carbon ($C\alpha$) atoms RMSD of the different systems for the full protein excluding flexible loops (residues with RMSF larger than 2.5 Å). Each of the five simulations was run until the RMSD remained stable and was then extended for another 100 ns, or 50 ns in the case of the H1047R holo mutant structure; these were considered as a production run. Moreover, we monitored the stability of the $C\alpha$ RMSD of the kinase domain, where the PIK-108 inhibitor binds. Finally, we examined the interaction energies between p110 α and niSH2 over the production runs.

Trajectory snapshots were saved every 2 ps during production simulations. The analysis of the trajectories was performed using GROMACS tools v4.5.4³⁶ and the Hydrogen Bond and Salt Bridges plugins of VMD.⁴⁶ VMD was also used to visualize trajectories and to produce Figures 1–6 and Figures S6, S8, and S9 (Supporting Information). Chimera was used for the preparation of holo systems (see above).³⁵ Plots were prepared with the GRaphing, Advanced Computation and Exploration (GRACE) program⁴⁷ and MATLAB.⁴⁸

In order to obtain representative conformations of the five simulated proteins, the trajectories were clustered by performing two separate cluster analyses using the gromos algorithm.⁴⁹ The first cluster analysis was applied on the whole protein, and the second was focused on the kinase domain (residues 697–1068). The highly flexible loop residues 1–7, 231–240, 291–330, 410–417, 505–530, 863–872, 941–952, and 1047–1068 were excluded from the calculations. Different cutoff values in the range between 1.0 and 1.5 Å were tested in each case; the final values were chosen on the basis of those that produced balanced cluster sizes (Table S1, Supporting Information). The first kinase cluster representatives were used to predict possible binding pockets using the FTMap web server.³⁴

Principal component analysis (PCA) was performed on the kinase domain (residues 697–1068). PCA of an MD trajectory, also known as essential dynamics, is a technique routinely used to separate large-scale correlated motions in a system from random thermal fluctuations.^{50,51} PCA is a standard mathematical tool used to detect correlations in large data sets; it

consists of a linear transformation that converts a set of potentially correlated variables into a set of uncorrelated variables called principal components or PCs that characterize motions of flexible regions in proteins, taking into account anharmonic effects. The first PC accounts for the largest variation in protein movement, and each of the succeeding PCs accounts for as much of the remaining variation as possible. Practically, low frequency modes reflect large collective motions of the protein and high frequency motions correspond to small local fluctuations (e.g., bond vibrations). Using this technique, one can extract the functionally relevant low frequency motions from a simulated MD trajectory and link those to the protein conformational dynamics, which in turn are linked to its function. Importantly, the dynamics along the individual modes of motion can be inspected and visualized separately. In the analysis performed herein, only the $C\alpha$ coordinates were used. Flexible loops not connected to functionally important regions of the protein (residues with RMSF larger than 2.5 Å) were excluded from the calculations in order to extract functionally relevant low-frequency motions.⁵² These loops encompass residues 863–872, 941–952, and 1047–1068. The g_covar and g_anaeig GROMACS tools were used for the calculation of the covariance matrix and the PCs, respectively. For the calculation of the covariance matrix, the trajectories were first projected onto the first 10 PCs of the respective systems. The choice of the first 10 principal components of the trajectory was made, as these eigenvectors represent 80–90% of the total motion (depending on the simulated system).⁵³

2.4. In Vitro Assays. PI3K α activity assays were performed using PIP2 containing liposomes prepared as previously mentioned in ref 54. Complexes of PI3K3CA (WT or H10147R)/PIK3R1 were obtained from Millipore. The assay was based on a protocol provided by Millipore, with modifications (Papafotika et al., in preparation). In this assay, PIP3 molecules produced by PI3K α compete with biotinylated PIP3 for binding with recombinant GST-GRP1-PH domain (amino acids 263–380), which has been produced in bacteria,⁵¹ bound to glutathione coated 96-well plates. Quantitation of the competed amount of biotin-PIP3 is estimated by the peroxidase activity of streptavidin-HRP that binds to the plate and provides a measure for the activity of the protein. The inhibitors, PIK-108 or wortmannin, are preincubated with all the components of the assay mixture, except PIP2, for 10 min, at 25 °C. PIP2 is added in the end of the preincubation period, thereby initiating the kinase reaction. IC50 values were calculated from dose–response curves using logit-log plots. All assays were carried out in at least three independent experiments and each concentration in triplicate. PIK-108 was a kind gift of Elias Couladouros (Agricultural University of Athens, Greece). Wortmannin was bought from Sigma-Aldrich.

3. RESULTS AND DISCUSSION

3.1. System Equilibration and Stability of PIK-108 in Two PI3K α Pockets. The RMSD for the $C\alpha$ atoms for all five simulations was calculated in order to monitor structural variations over the time course of the simulations and to obtain an overall indication of the stability of each system. Figure S1 (Supporting Information) indicates that a plateau is reached at different time points for each simulation. Hence, the trajectories that were considered as production runs and were used for further analysis were the following: 90–190 ns for the human WT holo (hWT-holo), 40–140 ns for murine WT holo (mWT-holo), 210–260 ns for the human H1047R mutant holo

(hMUT-holo), 150–250 ns for the human WT apo (hWT-apo), and 50–150 ns for the human H1047R mutant apo (hMUT-apo) proteins (Table 1). Production runs are thus 100 ns with the exception of the human H1047R mutant holo, where the production run is 50 ns as its total $C\alpha$ RMSD showed an increasing trend during 0–210 ns. However, the RMSD of the $C\alpha$ carbons of the kinase domain, where all analyses were performed herein, indicates that this domain remains stable after the first 25 ns of the simulation for all systems (Figure S2, Supporting Information). As an additional metric for system equilibration, we calculated the time series of the interaction energies between (a) the catalytic subunit p110 α and the regulatory subunit niSH2 domain (Figure S3, Supporting Information) and (b) PIK-108 and the protein in the ATP and non-ATP pockets (Figure S4, Supporting Information) throughout the production run. These results show that the interaction energies between different components of the system remain stable. Finally, comparison between the first cluster representative of the murine WT holo simulation and its respective crystal structure (PDB ID: 4A55)²⁰ results in an overall $C\alpha$ RMSD (not including flexible loops) of 1.9 Å (Figure 2, top), indicating that the used protocol and force field are appropriate for the present study.

The stability of PIK-108 in terms of binding to the two pockets is demonstrated in both the ATP and non-ATP

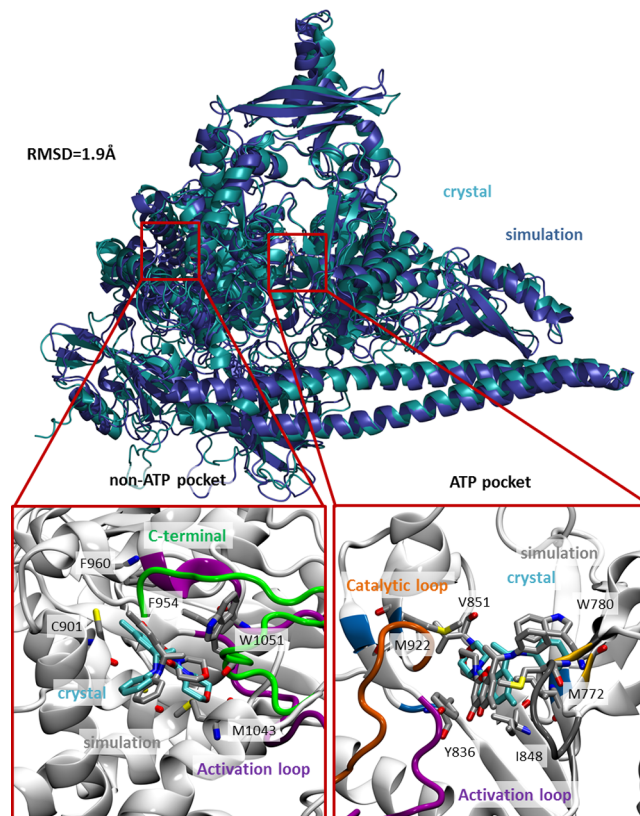


Figure 2. Center top: Overlap between the murine WT PI3K α crystal structure (cyan)²⁰ and the first cluster representative (blue) from the simulations performed herein. Bottom left: Snapshot of the first cluster representative for the non-ATP pocket shown in gray. The overlap with the cocrystallized PIK-108 taken from ref 20 is shown in cyan. Bottom right: Snapshot of the first cluster representative for the ATP pocket shown in gray. The overlap with the cocrystallized PIK-108 is shown in cyan. Interacting PI3K α residues with PIK-108 are labeled.

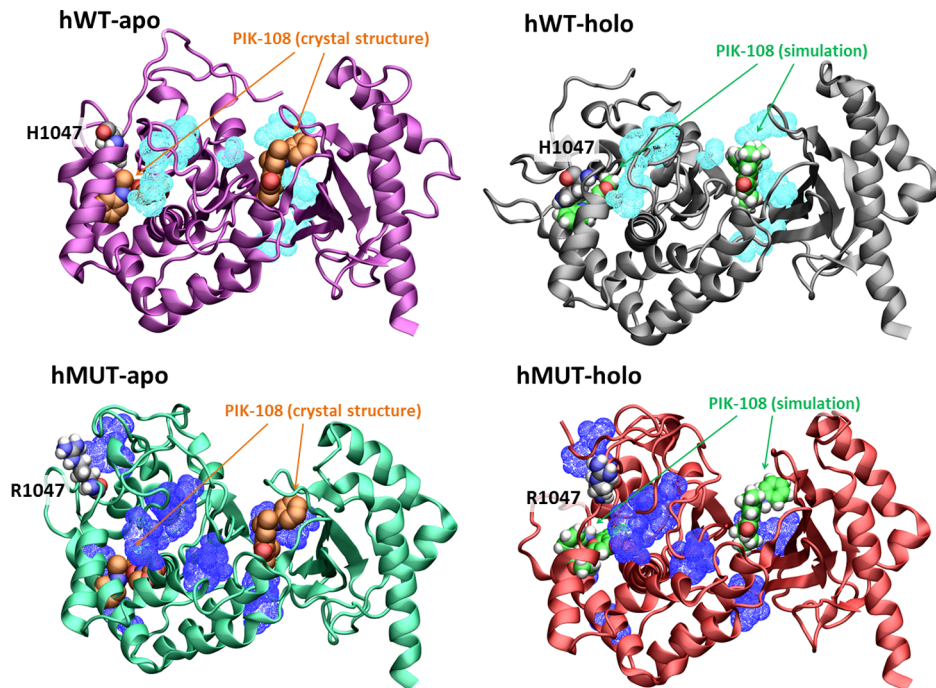


Figure 3. Binding site prediction results. First cluster representatives from the hWT- and hMUT-apo (left) and hWT- and hMUT-holo (right) trajectories are depicted in purple (hWT-apo), green (hMUT-apo), gray (hWT-holo), and red (hMUT-holo) cartoon representations. Residue 1047 is shown in VDW representation and colored by atom type (carbon is shown in gray). Dots represent predicted binding sites identified by the FTMap server for the apo proteins. PIK-108 from the crystal structure 4A55 is also shown in VDW representation and colored by atom name (carbon is shown in orange) after aligning the cluster representatives with the 4A55 crystal structure (left). PIK-108 in the holo forms corresponds to the first cluster representatives from the simulations of hWT-holo and hMUT-holo and is also shown in VDW representation and colored by atom name (carbon is shown in green) (right).

pockets through the interaction energies between PIK-108 and neighboring residues in all three PI3K α variants (mWT, hWT, hMUT) (Figure S4, Supporting Information). Moreover, we calculated the RMSD of the $C\alpha$ carbons of the residues lining the two pockets, namely, 772, 780, 800, 836, 922, 930, 851, 848, 770, 778, 850, 932, and 933 for the ATP pocket and 954, 955, 956, 957, 1043, 1044, 984, 1047, 1051, 960, 964, 977, 980, and 981 for the non-ATP pocket. These residues appear in at least one of the protein variants within a distance of 5 Å from PIK-108. The RMSD of these residues is shown in Figure S5 (Supporting Information). The stability of the ligand RMSD in the ATP pocket indicates that in both hWT and hMUT variants inclusion of PIK-108 does not promote any dramatic changes in the catalytic site. On the contrary, binding of PIK-108 in the inherently more flexible non-ATP pocket leads to a conformational change in the vicinity of PIK-108, which is stabilized after approximately 60 and 150 ns for the hWT and hMUT proteins, respectively. This conformational change close to the non-ATP pocket of the hWT involves the movement of the C-terminal tail of the protein (res. 1047–1068) from an extended conformation that points toward the ATP pocket in the apo simulation to being more compact and closer to $\kappa 11$ helix (res. 1031–1047) [videos S1 (jp506423e_si_002.mpg) and S2 (jp506423e_si_003.mpg), Supporting Information]. In the case of hMUT, the main conformational change evolving through the first 150 ns of the simulation upon ligand binding is the movement of the activation loop close to PIK-108 (the overall $C\alpha$ RMSD of the activation loop between the apo and holo structures is 8 Å), as well as the opening of the non-ATP pocket by the movement of $\kappa 11$ helix and the C-terminal tail. These changes are elaborated below.

3.2. The Effect of PIK-108 Binding on Protein Structure.

3.2.1. Binding Site Identification. In order to investigate whether the newly discovered non-ATP site on the murine PI3K α could be viable on the human WT and mutant H1047R PI3K α , we performed binding site identification with FTMap³⁴ on the first cluster representatives of the kinase domains of the two apo proteins (see the Methods). The results are presented in Figure 3. To illustrate the relative position of PIK-108 and the predicted binding sites of the hWT and hMUT, apo and holo proteins, we have depicted (i) the first cluster representatives of the apo structures with the PIK-108 of the mWT crystal structure, after aligning with the $C\alpha$ carbons of the nonflexible loops (Figure 3, left), and (ii) the first cluster representatives of the holo structures, including the PIK-108, and the binding sites as predicted for the apo proteins (Figure 3, right). As seen in Figure 3, the existence of the novel non-ATP binding pocket in the proximity of residue 1047 as well as of the active site in both the hWT and mutant proteins is predicted by FTMap. The predicted pockets on the cluster representatives of the apo hWT and hMUT proteins are close to the position of PIK-108 in the experimental structure after overlapping with the murine WT crystal structure (Figure 3, left). Additionally, in the mutant H1047R PI3K α , a binding pocket in the vicinity of the mutated residue Arg1047 was identified (Figure 3, bottom left). The predicted binding sites are also close to the position of PIK-108 from the simulations of the holo protein proteins. Interestingly, despite the fact that the predicted sites close to residue 1047 for both hWT-apo and hMUT-apo forms occupy similar areas, the chemistry of the FTMap probes that bind there is different. This result is illustrated in Figure S8 (Supporting Information) where the

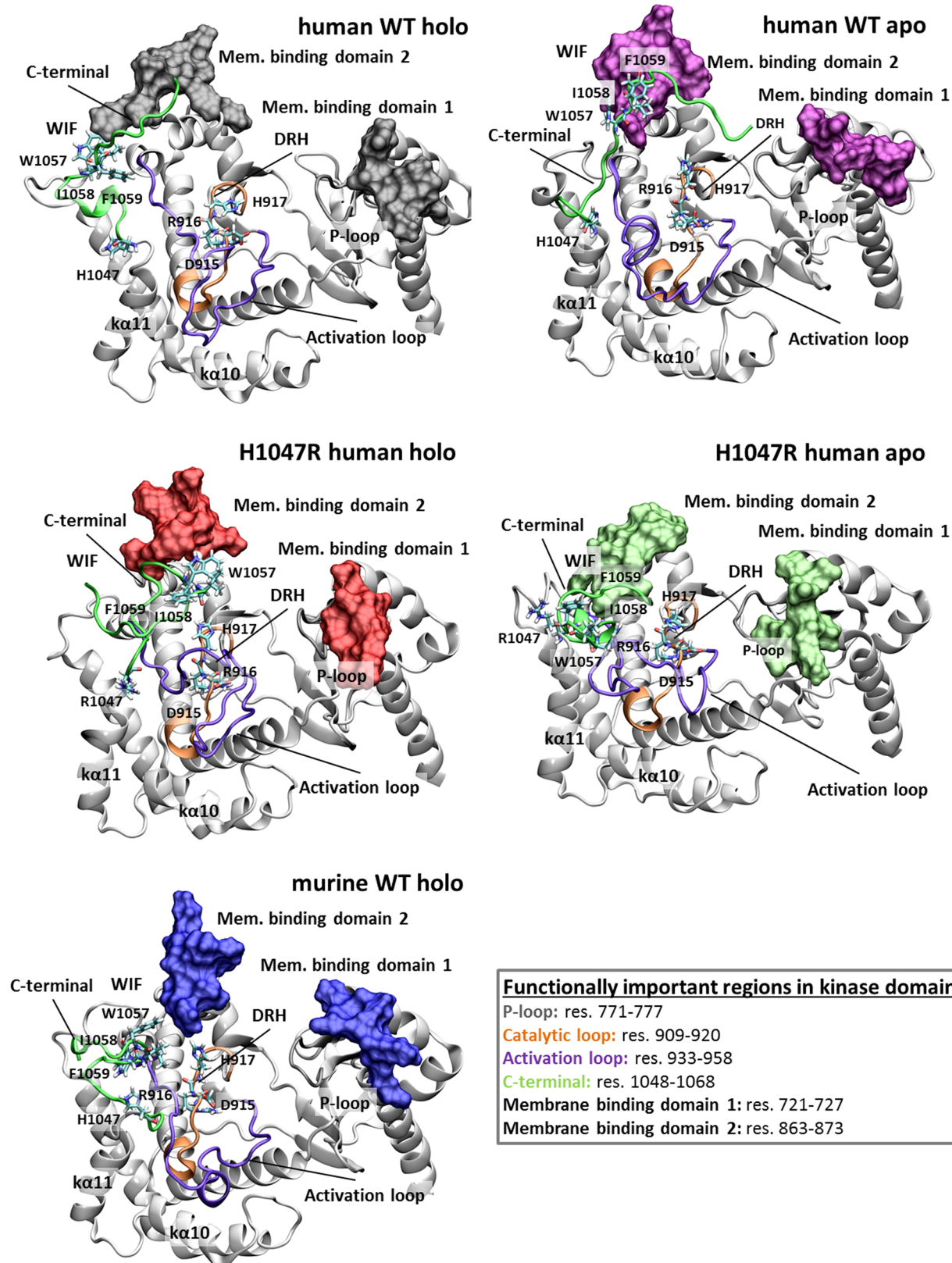


Figure 4. First cluster representatives of the kinase domain. Functional loops are labeled to illustrate differences among protein forms.

predicted sites are colored by probe type and could be used as a guide in the design of mutant-specific binders that interact with the mutated residue. To further assess the effect of PIK-108 binding in the kinase domain, we monitored structural variations among the five protein forms.

3.2.2. Comparison between Cluster Representatives. To investigate structural differences between the five different protein states (hWT-apo, hMUT-apo, mWT-PIK108, hWT-PIK108, hMUT-PIK108), we compared the first cluster representative conformations from each simulation (Figure 4

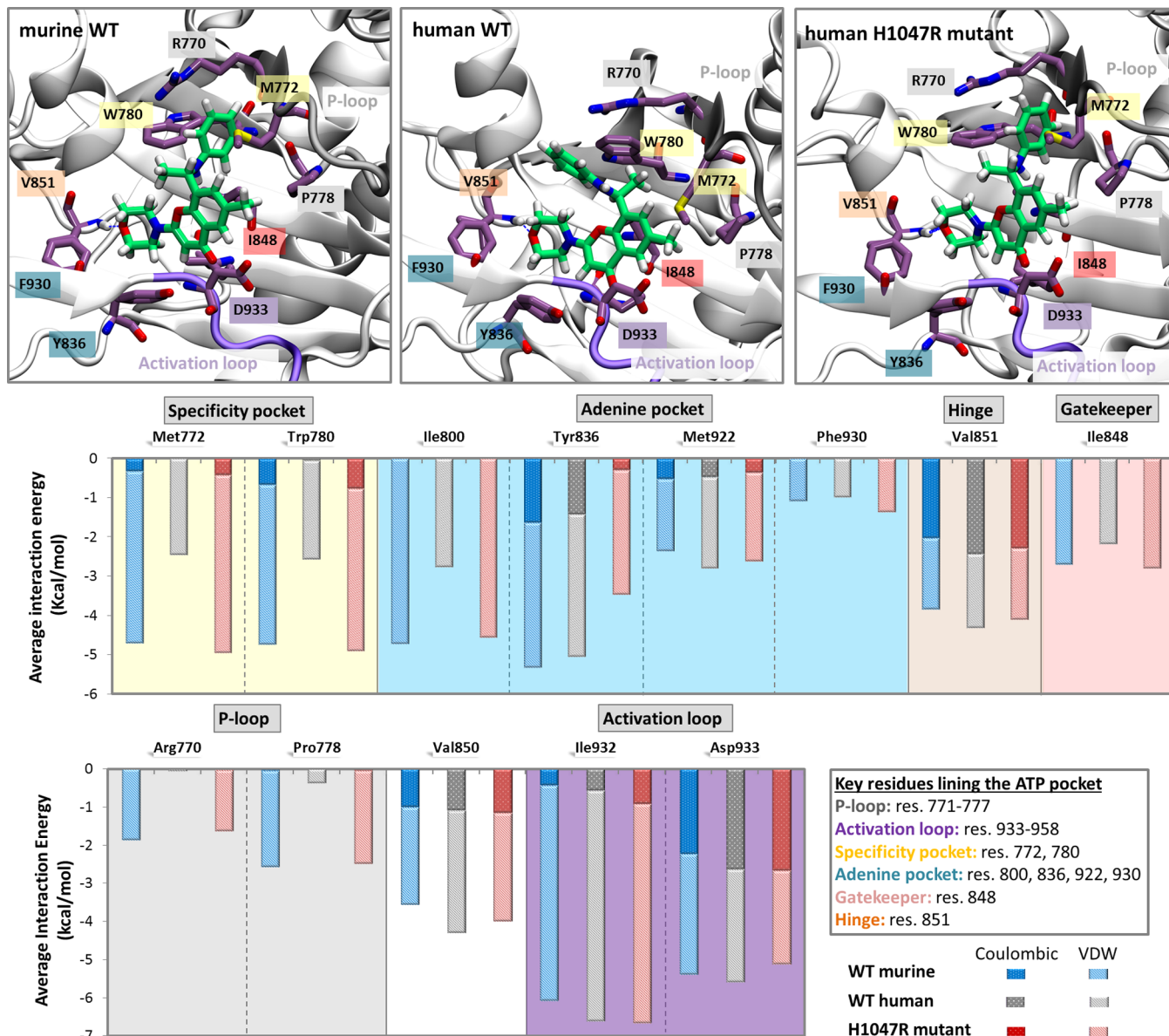


Figure 5. Top: PIK-108 binding in the ATP pocket of the first cluster representatives for the mWT, hWT, and hMUT. Center/bottom: interaction energies of PIK-108 with key residues lining the ATP pocket. Each bar is divided in the Coulombic and van der Waals components indicated by darker and lighter colors, respectively. Blue corresponds to the mWT, gray to hWT, and red to hMUT H1047R.

and Figure S6, Supporting Information). Comparison of the apo and holo human WT structures as well as the apo and holo mutant PI3K α structures based on the kinase domain shows that the major difference upon compound binding in these proteins lies in the vicinity of membrane binding domain 1 (res. 721–727), membrane binding domain 2 (res. 863–873), and the $\kappa 7/\kappa 8$ elbow (res. 966–974), as can be seen in Figure 4 and Figure S6 (Supporting Information); these areas have been proposed to act as membrane binding domains.⁵⁵

More specifically, the RMSD between the $C\alpha$ of the hWT-apo and -holo forms for the membrane binding domain 1 is 3.69 Å, while that between the mutant apo and holo forms is 5.07 Å, indicating that the effect of PIK-108 binding is more pronounced in the case of the mutant protein. Comparison between the mWT-holo with the rest of the protein variants gives rise to an RMSD in the range of 3.83–6.74 Å. Interestingly, the $C\alpha$ RMSD between the hWT-apo and

hMUT-apo proteins is 9.78 Å, demonstrating that the two proteins are significantly different in this area.

Structural differences upon compound binding are also observed in membrane binding loop 2 (res. 863–873), which significantly changes its conformation, as can be seen in Figure 4, with the difference being more pronounced in the case of the human mutant protein. The RMSD of the $C\alpha$ of the WT apo and holo forms for the membrane binding loop 2 is 7 Å, while for the mutant apo and holo forms it is 13.7 Å. Notably, the conformation of the membrane binding loop 2 of the holo mutant form resembles the conformation of the murine WT counterpart with their $C\alpha$ RMSD being 5.6 Å. On the other hand, the human WT holo structure of the membrane binding loop 2 maintains a much different conformation from the murine WT holo structure with their $C\alpha$ RMSD being 11 Å. It should be noted that the RMSF fluctuations of the membrane binding loop 1 and membrane binding loop 2 are similar (Table S3, Supporting Information).

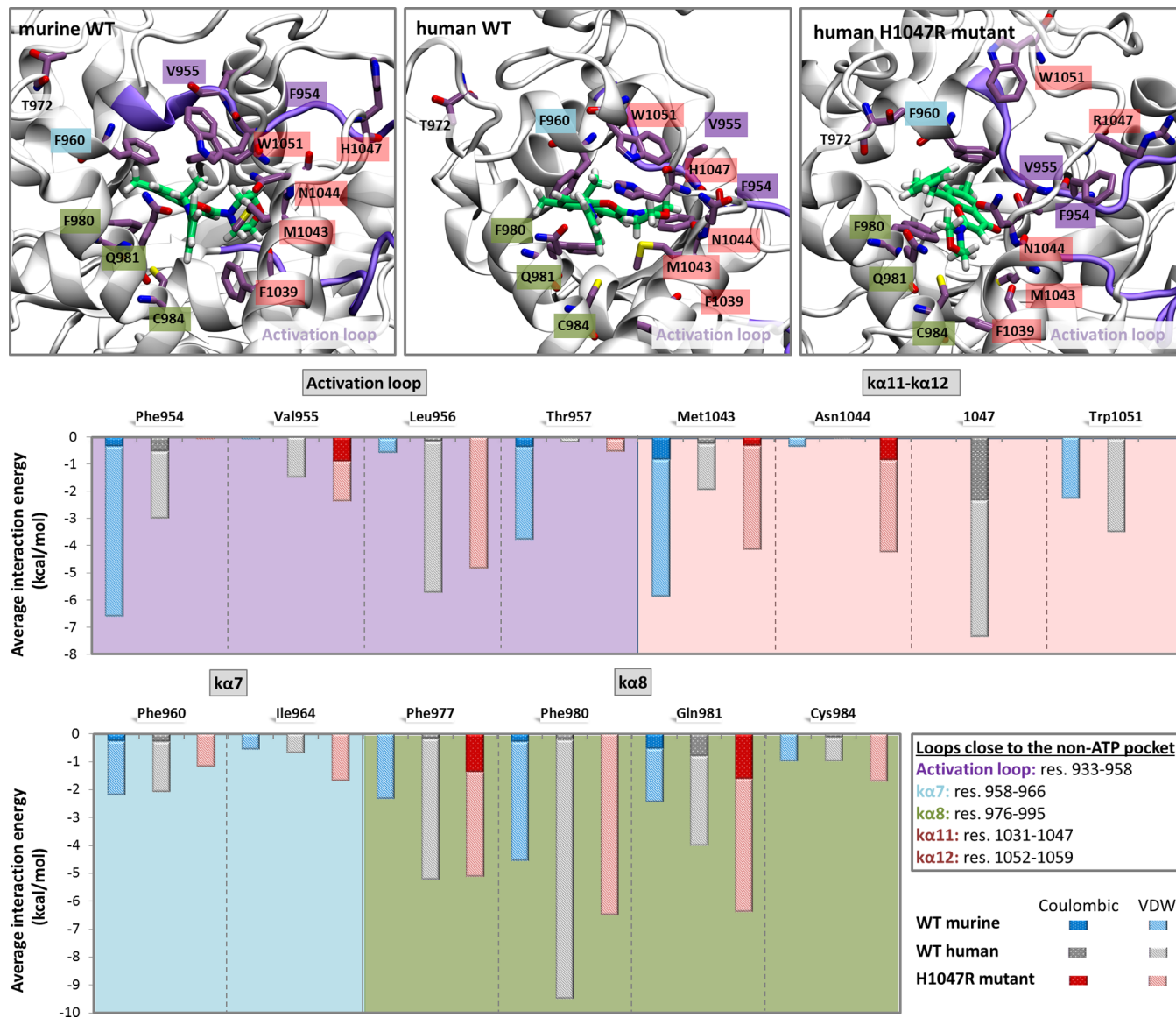


Figure 6. Top: PIK-108 binding in the non-ATP pocket of the first cluster representatives for the WT murine, WT human, and H1047R mutant. Center/bottom: interaction energies of PIK-108 with key residues close to the pocket.

The differences among the different protein variants are more pronounced in the k α 7/k α 8 elbow (Figure S6, Supporting Information). The k α 7/k α 8 elbow RMSD of 10.92 Å between mWT-holo and hWT-holo structures indicates that this specific region adopts a significantly different conformation. The difference in the conformation of the k α 7/k α 8 elbow is less pronounced between the mWT-holo and the three remaining variants, i.e. hWT-apo, hMUT-apo and hMUT-holo, as indicated by the RMSD values in Figure S6 (Supporting Information). This change in conformation of the k α 7/k α 8 elbow upon PIK-108 binding in the hWT is also demonstrated by the RMSD value between hWT-apo and -holo forms, which is 11.96 Å (Figure S6, Supporting Information). This effect is less intense in the case of hMUT, where the RMSD of the k α 7/k α 8 elbow between the apo and holo forms is 6.12 Å. We also monitored structural changes of other functionally important structural elements of the kinase domain such as the P-loop, activation and catalytic loops, C-terminus (C-ter), and the hotspot residue 1047 (shown in Figure 4). We observe that, upon compound binding on the H1047R human

mutant, the catalytic loop retains the same conformation with its C α RMSD between the complexed and uncomplexed forms being a mere 1.6 Å, while the activation loop changes its conformation significantly (C α RMSD = 8.1 Å). The activation loop contacts helix k α 12 in the apo form, and upon compound binding, it is shifted toward the ATP pocket. Moreover, the P-loop in the two protein forms has a C α RMSD of 5.4 Å and is shown to retain a more closed conformation in the apo simulation, which is expected as in the case of the holo simulation, where the P-loop is shifted away from the active site to accommodate the ligand. Mutated residue Arg1047 in the apo form points toward the C-terminal tail and is implicated in hydrophobic contacts with residue Phe1059 of the WIF motif (res. 1057–1059) as well as cation–π interactions with Trp1051. In the hMUT-holo protein, these interactions are not observed and Arg1047 is orientated toward helix k α 11, forming a frequent hydrogen bond with the side chain of Asp1045 (67% frequency). Other structural elements of the kinase domain, i.e., the catalytic loop (res. 909–920), the activation loop (res. 933–958), and the P-loop (res. 771–777),

do not present significant differences between the apo and holo mutant PI3K α .

In the case of the hWT-holo and -apo simulations, compound binding does not influence greatly the conformation of the catalytic loop ($C\alpha$ RMSD = 2.1 Å) as in the case of the hMUT simulation ($C\alpha$ RMSD = 1.6 Å), while the activation loop changes its position ($C\alpha$ RMSD = 4.9 Å). As observed in the hMUT protein simulations, the P-loop opens in the holo form to accommodate the ligand in comparison to the apo form ($C\alpha$ RMSD of 2.8 Å). In the hWT simulation bound to PIK-108, His1047 interacts significantly with the compound, changing its position and interactions with neighboring residues compared to the apo form. Specifically, while in the hWT-apo form His1047 is hydrogen bonded to Leu956, in the holo PI3K α the side chain of His1047 forms a hydrogen bond with the backbone of Gly1049, and the backbone His1047 hydrogen bonds to the backbone of Met1055. It should also be noted that the C-ter of the WT protein in the apo form blocks the entrance to the catalytic site coming close to the P-loop, while in the other protein structures (holo forms of mWT, hWT, and hMUT and apo form of hMUT) the C-ter is coiled and does not interact with the vicinity of the active site [Figure 3, Figure S6 (Supporting Information), and videos S1–S5 (jp506423e_si_002.mpg to jp506423e_si_006.mpg) (Supporting Information)]. In agreement with experimental studies, the WIF motif (res. 1057–1059), depicted in Figure 4, performs stacking interactions.²⁰ The WIF motif is conserved as a triplet of hydrophobic residues in class I and class II PI3Ks and is required for protein binding to anionic lipids through the C-ter tail.²⁰ As observed in Figure S7 (Supporting Information), Trp1057 (W) stacks ideally with Ile1058 (I) in the case of the hWT-holo, hMUT-holo, and apo forms throughout the production run, while Ile1058 (I) stacking with Phe1059 (F) is partly perturbed in the simulations of hWT-holo, hMUT-holo and -apo, and mWT proteins. The hWT-apo form maintains relatively long distances between the residues comprising the WIF motif (4–10 Å, Figure S7, Supporting Information).

3.3. PIK-108–Protein Interactions. **3.3.1. Protein–Ligand Interactions in the ATP Binding Pocket.** Within the catalytic site, PIK-108 packs between p110 α residues Ile800, Val850, and Val851 on one side and residues Met922, Phe930, Ile932, and Asp933 on the other side (as observed in the X-ray structure²⁰) throughout the course of the simulation for all systems. In Figure 5, PIK-108 binding in the ATP pocket is shown for the first cluster representatives for the WT murine, WT human, and H1047R mutant PI3K α . The interaction energies of PIK-108 with key residues lining the ATP pocket were monitored in the three protein forms (Figure 5, bottom). The compound remains stable in the ATP pocket throughout the simulation and is stabilized by similar interactions in all three protein variants. The key hydrogen bond with Val851 stabilizes the ligand positioning in the catalytic pocket and is observed at 88% frequency in the mWT, 92% in the hWT, and 91% in the hMUT. Interestingly, the PIK-108 pose is almost identical in the case of mWT and hMUT with an RMSD of 1.25 Å, whereas the RMSD between the mWT and hWT is 2.89 Å (Figure S9, Supporting Information, the RMSD of PIK-108 is calculated after alignment of the residues lining the ATP pocket). The PIK-108 aminobenzene ring forms T-shape π – π interactions with Trp870 in the case of mWT and hMUT, while in the hWT protein the aminobenzene group rotates by 90° and interacts with Trp780 through off-parallel π – π interactions.

Moreover, due to this 90° rotation of the aminobenzene ring in the case of hWT, PIK-108 does not interact with P-loop residues Arg770 and Pro778. These findings are confirmed by monitoring the interaction energies (Figure 5, bottom), which show that the mWT and hMUT proteins form similar interactions with the specificity pocket and the P-loop (res. 771–777), while these interactions are either lower or absent in the case of hWT.

3.3.2. Protein–Ligand Interactions in the Non-ATP Binding Pocket. PIK-108 interacts with residues of the non-ATP site gorge ranging from Cys905 at the bottom to Trp1051 at the top (Figure 6 and Table S2, Supporting Information). Five of these residues are aromatic and are involved in complementary surface contacts with the ligand (Phe909, Phe977, and Phe980) as well as stacking interactions (Phe954 and Phe960). Despite the structural similarity of the κ 8 (res. 976–995) and κ 11 (res. 1031–1047) helices in the three protein structures, the difference in the conformation of the activation loop (res. 933–958) and κ 12 (res. 1052–1059) leads to three different poses and interaction patterns for each respective system. In the hWT, the ligand strongly interacts with Phe980 from the κ 8 helix and His1047. These two interactions influence PIK-108 orientation in the pocket by stacking with its morpholino group and changing the overall pose of the ligand compared to the other two protein forms. On the contrary, interaction of PIK-108 with the mutated residue Arg1047 was not observed in the case of the mutant. Instead, Arg1047 forms a salt-bridge with the Asp1045, which keeps Arg1047 away from the non-ATP pocket. Because of the different conformation of κ 12 in the H1047R mutant, Trp1051 is located far from the pocket, while in both WT forms it interacts with the methyl group of PIK-108. Similarly, the interaction of PIK-108 with Phe954 from the activation loop is absent from the mutant form. Conclusively, while the interactions of the ligand PIK-108 are similar in the ATP pocket of the three protein structures, the interactions in the non-ATP pocket are markedly different between the mWT, hWT, and hMUT.

3.4. The Effect of PIK-108 Binding on Protein Dynamics. **3.4.1. Principal Component and Covariance Analysis.** Allosteric modulators typically bind to less conserved sites compared to the active site of an enzyme and may confer greater specificity in protein kinase regulation.^{7–9} Unlike ATP-competitive inhibitors, allosteric modulators bind outside the catalytic pocket and modify kinase activity by altering the protein conformational landscape.^{24,25,56–58}

In proteins, local fluctuations and collective motions occur simultaneously, which makes it hard to distinguish the two types of motion from each other. Principal component analysis (PCA) can help in such cases, as it can filter global, collective (often slow) motions from local, fast motions. PCA was used herein to investigate the dominant motions of the three proteins in their apo and holo forms and the implication of the newly discovered non-ATP site in allosteric regulation of PI3K α .

The first three principal components (PCs), representing the first three dominant kinase motions for the five simulated systems, are shown in videos S6–S20 (jp506423e_si_007.mpg to jp506423e_si_021.mpg) (Supporting Information). Our analysis shows that the systems studied in the present work can be classified in two groups depending on the dominant motion that they perform (kinase twisting and hinge-bending motions). We found that the dynamics of the mWT-holo structure

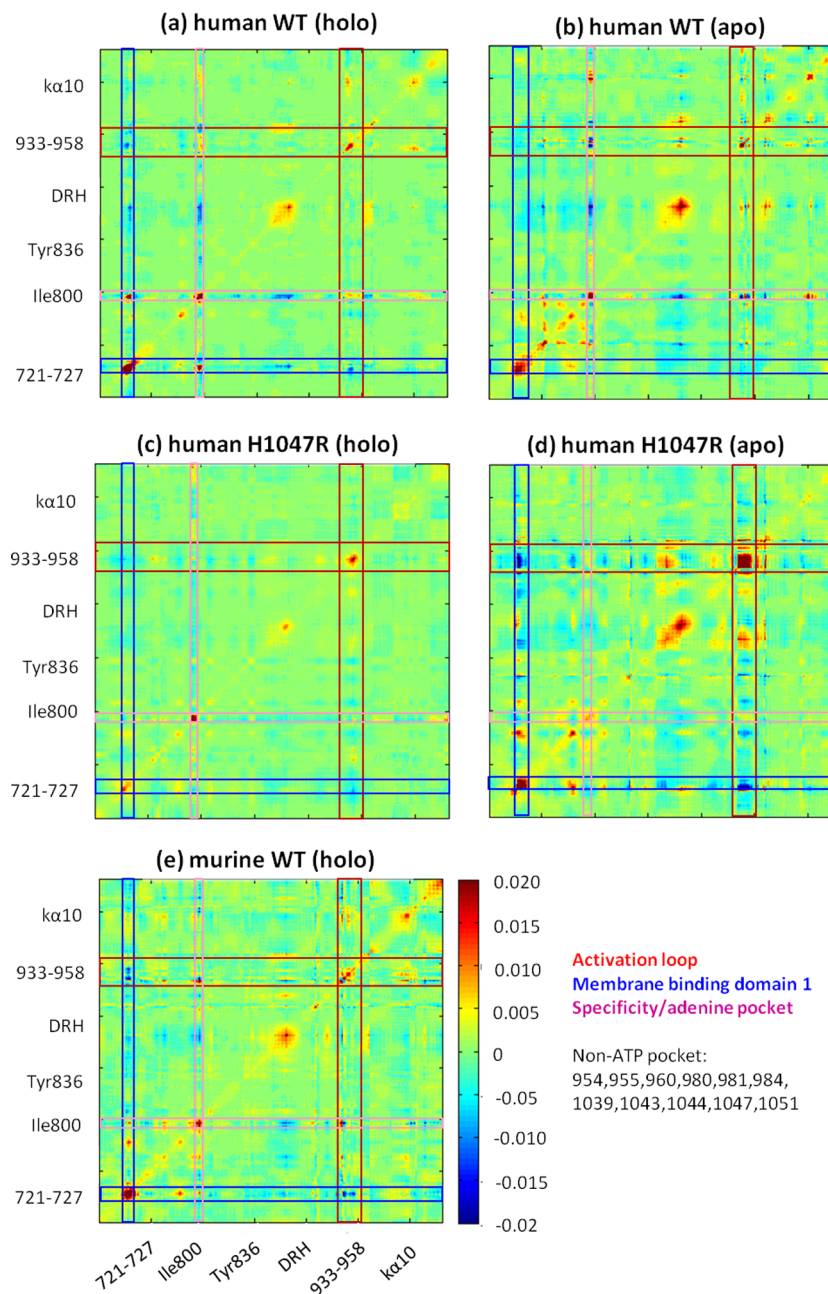


Figure 7. Positional covariance matrices of the kinase domain for the different systems of the proteins: (a) human WT holo, (b) human WT apo, (c) human mutant holo, (d) human mutant apo, and (e) murine WT holo. Only nonflexible loops have been considered. Activation loop, membrane binding loop 1, and specificity and adenine pocket residues are shown with red, green, and orange boxes, respectively.

resembles more those of the hWT-apo and hMUT-apo forms, as the dominant PC for these three protein systems is the twisting motion of the kinase domain, as shown in videos S6 (jpS06423e_si_007.mpg), S9 (jpS06423e_si_010.mpg), and S12 (jpS06423e_si_013.mpg) (Supporting Information). On the contrary, in the case of the hWT-holo and hMUT-holo structures, PCA identifies as the protein dominant motion the hinge bending of the kinase domain [shown in videos S15 (jpS06423e_si_016.mpg) and S18 (jpS06423e_si_019.mpg), respectively, Supporting Information], while the twisting motion of the protein plays a secondary role; these results indicate that PIK-108 binding alters the protein dynamics.

To further elucidate the molecular basis of a possible allosteric communication between functional elements of

PI3K α and characterize the nature of collective motions between the different kinase regions, we further analyzed the positional covariance matrix of the protein kinase domains (Figure 7). The first striking result is that, for all simulations, motions of residues in the vicinity of the ATP pocket are not correlated to the motion of the non-ATP pocket, which implies that the non-ATP pocket may not participate in large scale motions affecting the catalytic site conformation. We thus hypothesize that this site may not be implicated in allosteric transitions of the enzyme via communicating with the catalytic pocket. Moreover, membrane binding domain 1 (res. 721–727) is anticorrelated with the specificity/adenine pocket of the active site in the hWT-apo and hMUT-apo and -holo proteins. The same domain is correlated with the active site residues in

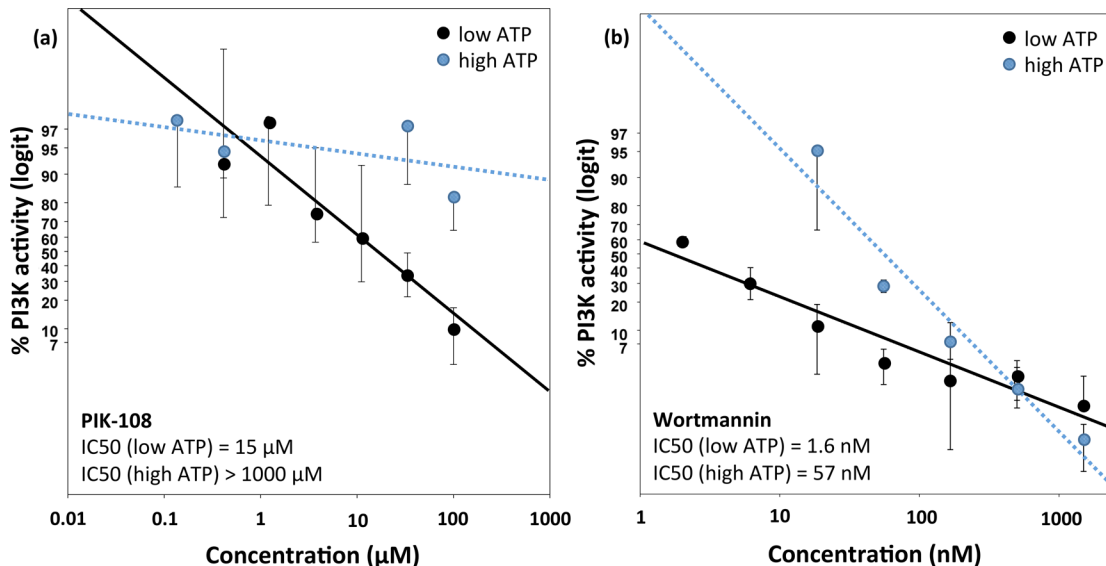


Figure 8. Competition between ATP and (a) PIK-108 and (b) wortmannin for the active site of PIK3CA. The activity of PIK3CA was assayed using a standard concentration of 100 μM ATP (solid symbols, black solid line) as well as a 20-fold higher concentration of ATP (2 mM, blue symbols, blue dashed line), at increasing concentrations of each compound. The IC₅₀s were estimated using the logit-log graph of SigmaPlot and linear regression analysis. Error bars show the standard error of the mean from at least three independent experiments, each one performed in triplicates. The IC₅₀s of both PIK-108 and wortmannin are dramatically altered in the presence of high ATP concentration, indicating that both compounds are competitive inhibitors of PI3K α .

the case of hWT-holo and mWT-holo structures. In all systems, the membrane binding loop 1 is also anticorrelated with the activation loop and the activation loop motion is correlated with the ATP pocket. Also, the specificity/adenine pocket residues are correlated with the C-lobe of the kinase and in particular with helix κ 10. For the hMUT-apo protein, the activation loop shows a strong correlation between itself in the form of concerted motions. Long-range cooperative interactions are observed only in the case of mWT-holo and between the P-loop and κ 8, κ 9, and κ 10 helices (Figure 7).

Calculation of the inner product of the PCs describing the hinge-bending and twisting motion of the kinase domain indicates that the modes of the protein are altered upon ligand binding. More specifically, in the case of hWT, the inner product of the PCs accounting for the hinge-bending motion (PC3 for the hWT-apo and PC1 for the hWT-holo) is 0.08, while the inner product for the PCs corresponding to the twisting motion (PC1 for the hWT-apo and PC2 for the hWT-holo) is 0.35. For the hMUT, the inner product between the PCs accounting for the hinge bending motion (PC3 for the hMUT-apo and PC1 for the hMUT-holo) is 0.44, whereas the inner product between PC1 of the hMUT-apo and PC3 of the hMUT-holo which correspond to the twisting kinase motion is 0.47. These results may be compared to five independent PI3K α trajectories that have been calculated each for the human WT and human mutant proteins. The inner product for the hinge-bending and twisting motions between trajectories of the same (uncomplexed) protein type is in the range 0.6–0.7.⁵⁴ Collectively, all the above data suggest that binding of PIK-108 to the non-ATP pocket does not influence the catalytic site conformation.

3.4.2. Root Mean Square Fluctuation Calculations. Root mean square fluctuation (RMSF) analysis of the MD trajectories reveals that certain regions important for enzyme function exhibit different and high mobility in the different PI3K α variants studied herein (Table S3, Supporting

Information), whereas others have similar flexibility but different conformation. The end of the C-terminal tail (res. 1048–1068) has high flexibility in all proteins and is more pronounced in both the apo and holo hWT forms, indicated both by the absolute value and the standard deviation of the RMSF. The activation loop (res. 933–958), catalytic loop (res. 909–920), and P-loop have not significantly altered mobility in the different protein forms. The membrane binding domain 1 (res. 721–727) is also influenced by PIK-108 binding. The effect of binding is inverse in the hWT and hMUT forms; the flexibility is increased in the hWT and decreased in the hMUT protein. Overall, PIK-108 binding limits the flexibility of hMUT, which is also in agreement with the covariance analysis (Figure 7, compare the left and right panels). Moreover, hMUT-apo and mWT-holo show very similar flexibility in the regions important for the enzyme function also in agreement with the PCA and covariance analysis.

3.5. In Vitro Biochemical Assays to Test the Allosteric Behavior of PIK-108. To test experimentally the computational finding that PIK-108 binding to the non-ATP pocket does not propagate any conformational information to the PI3K α active site, we assessed whether PIK-108 acts as an allosteric inhibitor of PIK3CA in an *in vitro* PI3K α activity assay, using as substrate PIP2 incorporated into liposomal membranes. To this end, we compared the IC₅₀ of the inhibition caused by PIK-108 at a commonly used concentration of ATP (100 μM) and at 20 times higher concentration (2 mM). The IC₅₀ of an allosteric inhibitor should remain unchanged and independent of the ATP concentration, while a competitive inhibitor will be influenced by the change in ATP concentration and may completely lose its activity.

Consistent with the computational data, a high concentration of ATP almost completely abolishes the inhibitory activity of PIK-108 (Figure 8A and Figure S10A, Supporting Information), suggesting that the inhibitory effect of this compound is solely due to its binding at the active site of PI3K α . As a

control, we tested the effect of a high concentration of ATP on the inhibitory effect of wortmannin, a known PI3K α inhibitor that binds covalently to the active site of the enzyme.⁵⁹ The high concentration of ATP increased 35-fold the IC₅₀ of wortmannin (from 1.6 to 57 nM), in accordance with binding of wortmannin at the active site of PI3K α (Figure 8B and Figure S10B, Supporting Information). Lack of complete abolishment of wortmannin inhibition may be attributed to the fact that wortmannin is a very strong inhibitor, which binds covalently the active site. In any case, since the concentration of ATP, in the competition experiment, has been raised 20-fold, the above increase of the IC₅₀ for wortmannin (35-fold) is within the expected range for an inhibitor that competes with ATP for the active site.

4. CONCLUSIONS

This article reports the first extensive MD simulations performed for three PI3K α forms (murine WT, human WT, and human H1047R mutant). The proteins were simulated complexed to a pan-PI3K inhibitor, PIK-108, which was recently reported to occupy a non-ATP pocket on the murine PI3K α , in addition to the catalytic site. In order to explore the existence of the non-ATP site in the human WT and human H1047R mutant proteins and its potential implication in allosteric modulation of PI3K α , we also modeled these proteins in the absence of the inhibitor and compared the complexed and uncomplexed protein structure and dynamics of these three protein forms.⁶⁰

First, we performed binding site identification on cluster representatives of the kinase domains of the human WT and mutant H1047R PI3K α in the apo and holo forms with FTMap.³⁴ After overlapping the human WT (hWT) and mutant H1047R (hMUT) PI3K α with their murine counterpart (mWT), we observe that the positions of PIK-108 in the murine PI3K α crystal structure largely overlap with the predicted positions from FTMap for both the catalytic and non-ATP pockets (Figure 3). By using MD simulations, we demonstrate that PIK-108 remains stable in both the ATP and non-ATP pockets in all three PI3K α forms (mWT, hWT, hMUT) by evaluating the RMSD of PIK-108 and the interaction energies between PIK-108 and neighboring residues. While residues in the vicinity of the non-ATP pocket are not correlated to the motions of the catalytic site, cluster analysis (Figure 4) in combination with the interaction energies of PIK-108 within the non-ATP pocket (Figure 6) indicates that upon binding of PIK-108 in the non-ATP pocket functionally important structural elements adopt altered conformations. PIK-108 binding induces a change in the C-ter position in the hWT simulation and the catalytic loop and C-ter conformations in the hMUT simulation, compared to the apo simulations. Part of the C-ter is lining the non-ATP pocket (residues 1043, 1044, 1047, and 1051), and thus, it is expected that the binding of PIK-108 will affect the C-ter conformation and interactions.

Structural comparison between the five protein states (hWT-apo, hMUT-apo, mWT-PIK108, hWT-PIK108, and hMUT-PIK108) reveals that the major difference upon compound binding in these proteins lies in the vicinity of membrane binding domain 1 (res. 721–727), membrane binding domain 2 (res. 863–873), and the $\kappa\alpha_7/\kappa\alpha_8$ elbow (res. 966–974), which have been proposed to act as membrane binding regions.⁵⁵ Although the C-ter is an inherently flexible element of these protein structures, we observed that, in hWT-apo

simulation, it blocks the entrance to the catalytic site and is proximal to the P-loop, while in the other protein structures (holo forms of mWT, hWT, and hMUT and apo form of hMUT) the C-ter is coiled and does not interact with the active site, which is in agreement with our previous studies.⁵⁴ Moreover, we observe that the membrane binding loop 1 is strongly anticorrelated with the activation loop in the hMUT simulation (Figure 7), which may be important for the H1047R mutant PI3K α overactivation mechanism, as it has been suggested that this mutant acts by changing the kinase interaction with the membrane.¹⁷ In agreement with experimental studies, the WIF motif (Figure 4), which is a key determinant in protein–lipid binding, performs stacking interactions observed in all simulations (Figure S7, Supporting Information),²⁰ though to a different degree. Overall, we observe a significantly diverse set of conformations upon ligand binding of the membrane binding loops 1 and 2, the $\kappa\alpha_7/\kappa\alpha_8$, and the WIF motif among the systems studied herein. On the basis of the implication of these regions in membrane binding, it can be postulated that these proteins will interact differently with the cell membrane depending on whether they are complexed or not with PIK-108.

In the catalytic site of the protein, PIK-108 remains stable throughout the simulation course and is stabilized by similar interactions in all three PI3K α variants with the key hydrogen bond to Val851 and other hydrophobic interactions stabilizing the ligand position. Although the PIK-108 pose as well as the interactions with the ATP pocket residues are almost identical when comparing the murine WT protein and the human mutant, there are marked differences between the murine and human WT proteins (Figure 5). PIK-108 remains stable throughout the production run also in the non-ATP pocket of PI3K α ; however, the interactions in this site are significantly different between the mWT, hWT, and hMUT proteins.

The notable differences between the three structures in the non-ATP pocket naturally prompt the question, “Is this new non-ATP pocket a possible allosteric site, and can it be exploited for allosteric modulation of PI3K α activity?” Allosteric modulators of protein function act by altering the conformational landscape of the protein and regulate protein activity by propagating these changes to the active site of the protein. We thus sought to explore whether the non-ATP pocket is conformationally linked to the catalytic site of the protein. In our quest, we first identified the dominant motions for each complexed and uncomplexed system through the first principal components (PCs) of the MD trajectory. We observed that the dominant motion of the protein is the twisting motion of the kinase domain in the case of the mWT-holo, hWT-apo, and hMUT-apo simulations, while, for the hWT-holo and hMUT-holo structures, PCA identifies as the protein dominant motion the hinge-bending of the kinase domain. Thus, it is evident that PIK-108 binding alters the dominant kinase motion between the apo and holo forms of the human WT and mutant PI3K α . Moreover, ligand binding freezes the correlations between the apo and holo forms (compare the left (holo) and right (apo) panels of Figure 7). However, investigation of the positional covariance matrix of the kinase domains indicated that the catalytic site is not positionally correlated to the non-ATP pocket, which implies that this newly identified pocket²⁰ may not participate in large scale motions affecting the catalytic site conformation. Moreover, the non-ATP pocket was not found to be correlated to other functionally important structural elements of PI3K α .

However, it should be noted that helix κ 12 as well as membrane binding loop 2 were excluded from the PCA analysis, as they were highly flexible (all other flexible loops that were not considered in the calculation are described in section 2.3); thus, no information can be derived from the positional covariance matrices for these structural elements. To test the hypothesis that the non-ATP site may not be implicated in allosteric transitions of the enzyme via communicating with the catalytic pocket, we performed cell-free *in vitro* assays in a standard ATP concentration as well as a high concentration of ATP. We find that, in agreement with the computational data, a high concentration of ATP almost completely abolishes the inhibition of PIK-108, suggesting that its inhibitory effect is due to binding to the active site of PI3K α and thus it may not be considered as an allosteric inhibitor.

A striking, yet not surprising, result is the fact that the main areas involved in protein conformational changes upon ligand binding are the membrane binding domains. Thus, protein activity could, in the case of PI3K α , be altered not only in terms of the active site availability but also by changing the motional components with which the protein interacts with the cell membrane and retrieves its substrate. Two literature references report the feasibility of targeting the protein–membrane interface;^{61,62} thus, the inhibition of protein–membrane interactions may represent a promising alternative or complementary strategy to targeting the catalytic site. In the case of PI3K α , PIK-108 is found in a non-ATP, nonallosteric binding pocket, which is adjacent to the site of the common H1047R mutant and on the protein surface that contacts the cell membrane. Since His-1047 of the WT PI3K α directly interacts with PIK-108 through π – π and electrostatic interactions (Figure 6), it could be envisaged that this non-ATP pocket could be utilized to develop a selective inhibitor of protein–membrane interactions tailored for the Arg-1047 mutant structure. Such an inhibitor could constrain the mobility of Arg-1047 or other membrane-binding motifs (such as WIF) and influence membrane accessibility and in turn substrate availability, since the H1047R mutation has been found to act by altering protein–membrane interactions.¹⁷ The impact of the H1047R mutation may also spread far beyond the immediate site of mutation, leading to functional changes in conformational mobility at other distant kinase regions, which may be the subject of future studies in the direction of uncovering H1047R-specific PI3K α inhibitors.

ASSOCIATED CONTENT

Supporting Information

Additional methodological details are provided. Supporting figures and tables indicating system equilibration and providing trajectory analyses are presented. Supporting videos showing the position of the C-terminal tail and the movement of the first three principal components of the kinase domain for the five protein systems are also provided. This material is available free of charge via the Internet at <http://pubs.acs.org>.

AUTHOR INFORMATION

Corresponding Author

*E-mail: zcournia@bioacademy.gr. Web: <http://www.drugdesign.gr>. Phone: +302106597195. Fax: +302106597545.

Notes

The authors declare no competing financial interest.

ACKNOWLEDGMENTS

The initial part of this work was cofunded by the NSRF 2007–2013, the European Regional Development Fund and national resources, under the grant “Cooperation” (No. 09ΣΥΝ 11-675). This work has also been supported by a Marie Curie Reintegration Grant (FP7-PEOPLE-2009-RG, No 256533) and an AACR Judah Folkman Fellowship for Cancer Research in Angiogenesis (08-40-18-COUR). We thank Dr. Roger Williams and Dr. Wai-Ching Hon for providing the coordinates of the murine PI3K α structure (PDB ID: 4A55) prior to official release from the Protein Data Bank. Part of the computational work was performed at BRFAA using a cluster funded from a European Economic Area Grant No. EL0084. We also acknowledge PRACE for awarding us access to the computational facility CURIE at GENCI@CEA, France. This work was also supported by the LinkSCEEM-2 project, funded by the European Commission under INFRA-2010-1.2.3, Grant Agreement No. RI-261600. We are grateful to Dr. Elias Couladouros and co-workers for providing the PI3K α inhibitor PIK-108. We thank Thomas Evangelidis for constructing the PI3K α models and Dr. Hari Leontiadou for the diligent proofreading of the manuscript and insightful discussions.

REFERENCES

- (1) Fruman, D. A.; Meyers, R. E.; Cantley, L. C. Phosphoinositide kinases. *Annu. Rev. Biochem.* **1998**, *67*, 481–507.
- (2) Vivanco, I.; Sawyers, C. L. The phosphatidylinositol 3-Kinase AKT pathway in human cancer. *Nat. Rev. Cancer* **2002**, *2*, 489–501.
- (3) Cantley, L. C. The phosphoinositide 3-kinase pathway. *Science* **2002**, *296*, 1655–1657.
- (4) Engelmann, J. A. Targeting PI3K signalling in cancer: opportunities, challenges and limitations. *Nat. Rev. Cancer* **2009**, *9*, 550–562.
- (5) Courtney, K. D.; Corcoran, R. B.; Engelmann, J. A. The PI3K pathway as drug target in human cancer. *J. Clin. Oncol.* **2010**, *28*, 1075–1083.
- (6) Knight, Z. A.; Gonzalez, B.; Feldman, M. E.; Zunder, E. R.; Goldenberg, D. D.; Williams, O.; Loewith, R.; Stokoe, D.; Balla, A.; Toth, B.; Balla, T.; Weiss, W. A.; Williams, R. L.; Shokat, K. M. A pharmacological map of the PI3-K family defines a role for p110alpha in insulin signaling. *Cell* **2006**, *125*, 733–747.
- (7) Simard, J. R.; Kluter, S.; Grutter, C.; Getlik, M.; Rabiller, M.; Rode, H. B.; Rauh, D. A new screening assay for allosteric inhibitors of cSrc. *Nat. Chem. Biol.* **2009**, *5*, 394–396.
- (8) Lindsley, C. W. 2013 Philip S. Portoghese Medicinal Chemistry Lectureship: Drug Discovery Targeting Allosteric Sites. *J. Med. Chem.* **2014**.
- (9) Changeux, J. P. The concept of allosteric modulation: an overview. *Drug discovery today. Technologies* **2013**, *10*, e223–228.
- (10) Samuels, Y.; Wang, Z.; Bardelli, A.; Silliman, N.; Ptak, J.; Szabo, S.; Yan, H.; Gazdar, A.; Powell, S. M.; Riggins, G. J.; Willson, J. K.; Markowitz, S.; Kinzler, K. W.; Vogelstein, B.; Velculescu, V. E. High frequency of mutations of the PIK3CA gene in human cancers. *Science* **2004**, *304*, 554.
- (11) Samuels, Y.; Diaz, L. A., Jr.; Schmidt-Kittler, O.; Cummins, J. M.; Delong, L.; Cheong, I.; Rago, C.; Huso, D. L.; Lengauer, C.; Kinzler, K. W.; Vogelstein, B.; Velculescu, V. E. Mutant PIK3CA promotes cell growth and invasion of human cancer cells. *Cancer Cell* **2005**, *7*, 561–573.
- (12) Saal, L. H.; Holm, K.; Maurer, M.; Memeo, L.; Su, T.; Wang, X.; Yu, J. S.; Malmstrom, P. O.; Mansukhani, M.; Enoksson, J.; Hibshoosh, H.; Borg, A.; Parsons, R. PIK3CA mutations correlate with hormone receptors, node metastasis, and ERBB2, and are mutually exclusive with PTEN loss in human breast carcinoma. *Cancer Res.* **2005**, *65*, 2554–2559.

- (13) Brana, I.; Siu, L. L. Clinical development of phosphatidylinositol 3-kinase inhibitors for cancer treatment. *BMC Med.* **2012**, *10*, 161.
- (14) Liu, S.; Knapp, S.; Ahmed, A. A. The structural basis of PI3K cancer mutations: from mechanism to therapy. *Cancer Res.* **2014**, *74*, 641–646.
- (15) Liu, P.; Cheng, H.; Roberts, T. M.; Zhao, J. J. Targeting the phosphoinositide 3-kinase pathway in cancer. *Nat. Rev. Drug Discovery* **2009**, *8*, 627–644.
- (16) Loibl, S.; von Minckwitz, G.; Schneeweiss, A.; Paepke, S.; Lehmann, A.; Rezai, M.; Zahm, D. M.; Sinn, P.; Khandan, F.; Eidtmann, H.; et al. PIK3CA mutations are associated with lower rates of pathologic complete response to anti-human epidermal growth factor receptor 2 (HER2) therapy in primary HER2-overexpressing breast cancer. *J. Clin. Oncol.* **2014**.
- (17) Mandelker, D.; Gabelli, S. B.; Schmidt-Kittler, O.; Zhu, J.; Cheong, I.; Huang, C. H.; Kinzler, K. W.; Vogelstein, B.; Amzel, L. M. A frequent kinase domain mutation that changes the interaction between PI3Kalpha and the membrane. *Proc. Natl. Acad. Sci. U. S. A.* **2009**, *106*, 16996–7001.
- (18) Huang, C. H.; Mandelker, D.; Schmidt-Kittler, O.; Samuels, Y.; Velculescu, V. E.; Kinzler, K. W.; Vogelstein, B.; Gabelli, S. B.; Amzel, L. M. The structure of a human p110alpha/p85alpha complex elucidates the effects of oncogenic PI3Kalpha mutations. *Science* **2007**, *318*, 1744–1748.
- (19) Zhang, X.; Vadas, O.; Perisic, O.; Anderson, K. E.; Clark, J.; Hawkins, P. T.; Stephens, L. R.; Williams, R. L. Structure of lipid kinase p110beta/p85beta elucidates an unusual SH2-domain-mediated inhibitory mechanism. *Mol. Cell* **2011**, *41*, 567–578.
- (20) Hon, W.-C.; Berndt, A.; Williams, R. Regulation of lipid binding underlies the activation mechanism of class IA PI3-kinases. *Oncogene* **2012**, *31*, 3655–3666.
- (21) Zhao, Y.; Zhang, X.; Chen, Y.; Lu, S.; Peng, Y.; Wang, X.; Guo, C.; Zhou, A.; Zhang, J.; Luo, Y.; Shen, Q.; Ding, J.; Meng, L. Crystal structures of PI3Kalpha complexed with PI103 and its derivatives: new directions for inhibitors design. *ACS Med. Chem. Lett.* **2014**, *5*, 138–142.
- (22) Wells, G. J. Allosteric modulators of G protein-coupled receptors. *Curr. Top. Med. Chem.* **2014**, *14*, 1735–7.
- (23) Nussinov, R.; Tsai, C. J. The design of covalent allosteric drugs. *Annu. Rev. Pharmacol. Toxicol.* **2014**.
- (24) Nussinov, R.; Tsai, C. J. The different ways through which specificity works in orthosteric and allosteric drugs. *Curr. Pharm. Des.* **2012**, *18*, 1311–1316.
- (25) Herbert, C.; Schieborr, U.; Saxena, K.; Juraszek, J.; De Smet, F.; Alcouffe, C.; Bianciotto, M.; Saladino, G.; Sibrac, D.; Kudlinzki, D.; et al. Molecular mechanism of SSR128129E, an extracellularly acting, small-molecule, allosteric inhibitor of FGF receptor signaling. *Cancer Cell* **2013**, *23*, 489–501.
- (26) Conn, P. J.; Lindsley, C. W.; Meiler, J.; Niswender, C. M. Opportunities and challenges in the discovery of allosteric modulators of GPCRs for treating CNS disorders. *Nat. Rev. Drug Discovery* **2014**, *13*, 692–708.
- (27) Zhang, J.; Adrin, F. J.; Jahnke, W.; Cowan-Jacob, S. W.; Li, A. G.; Iacob, R. E.; Sim, T.; Powers, J.; Dierks, C.; et al. Targeting Bcr-Abl by combining allosteric with ATP -binding-site inhibitors. *Nature* **2010**, *463*, 501–506.
- (28) Kruse, A. C.; Ring, A. M.; Manglik, A.; Hu, J.; Hu, K.; Eitel, K.; Hubner, H.; Pardon, E.; Valant, C.; Sexton, P. M.; et al. Activation and allosteric modulation of a muscarinic acetylcholine receptor. *Nature* **2013**, *504*, 101–6.
- (29) Changeux, J. P. 50 years of allosteric interactions: the twists and turns of the models. *Nat. Rev. Mol. Cell Biol.* **2013**, *14*, 819–829.
- (30) Jorgensen, W. L. The many roles of computation in drug discovery. *Science* **2004**, *303*, 1813–1818.
- (31) Jorgensen, W. L. Efficient drug lead discovery and optimization. *Acc. Chem. Res.* **2009**, *42*, 724–733.
- (32) Lamb, M. L.; Jorgensen, W. L. Computational approaches to molecular recognition. *Curr. Opin. Chem. Biol.* **1997**, *1*, 449–457.
- (33) Sali, A.; Blundell, T. Comparative protein modelling by satisfaction of spatial restraints. *J. Mol. Biol.* **1993**, *234*, 779–815.
- (34) Ngan, C. H.; Bohnnud, T.; Mottarella, S. E.; Beglov, D.; Villar, E. A.; Hall, D. R.; Kozakov, D.; Vajda, S. FTMAP: extended protein mapping with user-selected probe molecules. *Nucleic Acids Res.* **2012**, *40*, W271–W275.
- (35) Pettersen, E. F.; Goddard, T. D.; Huang, C. C.; Couch, G. S.; Greenblatt, D. M.; Meng, E. C.; Ferrin, T. E. UCSF Chimera—a visualization system for exploratory research and analysis. *J. Comput. Chem.* **2004**, *25*, 1605–1612.
- (36) Hess, B.; Carsten, K.; David, v. d. S.; Erik, L. GROMACS 4: algorithms for highly efficient, load-balanced, and scalable molecular simulation. *J. Chem. Theory Comput.* **2008**, *4*, 435–447.
- (37) Lindorff-Larsen, K.; Piana, S.; Palmo, K.; Maragakis, P.; Klepeis, J. L.; Dror, R. O.; Shaw, D. E. Improved side-chain torsion potentials for the Amber ff99SB protein force field. *Proteins* **2010**, *78*, 1950–1958.
- (38) Jorgensen, W. L.; Chandrasekhar, J.; Madura, J. D.; Impey, R. W.; Klein, M. L. Comparison of Simple Potential Functions for Simulating Liquid Water. *J. Chem. Phys.* **1983**, *79*, 926–935.
- (39) Sousa da Silva, A. W.; Vranken, W. F. ACPYPE - AnteChamber PYthon Parser interfacE. *BMC Res. Notes* **2012**, *5*, 367.
- (40) Wang, J.; Wang, W.; Kollman, P. A.; Case, D. A. Automatic atom type and bond type perception in molecular mechanical calculations. *J. Mol. Graphics Modell.* **2006**, *25*, 247–260.
- (41) Wang, J.; Wolf, R. M.; Caldwell, J. W.; Kollman, P. A.; Case, D. A. Development and testing of a general amber force field. *J. Comput. Chem.* **2004**, *25*, 1157–1174.
- (42) Essmann, U.; Perera, L.; ML, B.; Darden, T.; Lee, M.; Pedersen, L. A smooth particle mesh Ewald method. *J. Chem. Phys.* **1995**, *103*, 8577–8593.
- (43) Nose, S. A molecular dynamics method for simulations in the canonical ensemble. *Mol. Phys.* **1984**, 255–268.
- (44) Parrinello, M.; Rahman, A. Polymorphic transitions in single crystals: A new molecular dynamics method. *J. Appl. Phys.* **1981**, *52*, 7182–7190.
- (45) Hess, B.; Bekker, H.; Berendsen, H. J. C.; Fraaije, J. G. E. M. LINCS: A linear constraint solver for molecular simulations. *J. Comput. Chem.* **1997**, *18*, 1463–1472.
- (46) Humphrey, W.; Dalke, A.; Schulten, K. VMD: visual molecular dynamics. *J. Mol. Graphics* **1996**, *14*, 33–38.
- (47) GRaphing, Advanced Computation and Exploration (GRACE) program; Grace Development Core Team: 2011.
- (48) MATLAB 8.0 and Statistics Toolbox 8.1; The MathWorks, Inc: Natick, MA, 2013.
- (49) Daura, X.; Gademann, Jaun, B.; Seebach, D.; van Gunsteren, W.; Mark, A. Peptide folding: when simulation meets experiment. *Angew. Chem., Int. Ed.* **1999**, *38*, 236–240.
- (50) Garcia, A. E. Large-amplitude nonlinear motions in proteins. *Phys. Rev. Lett.* **1992**, *68*, 2696–2699.
- (51) Amadei, A.; Linssen, A. B.; Berendsen, H. J. Essential dynamics of proteins. *Proteins* **1993**, *17*, 412–425.
- (52) Hayward, S.; de Groot, B. L. Normal modes and essential dynamics. *Methods Mol. Biol.* **2008**, *443*, 89–106.
- (53) Chiappori, F.; Merelli, I.; Colombo, G.; Milanesi, L.; Morra, G. Molecular mechanism of allosteric communication in Hsp70 revealed by molecular dynamics simulations. *PLoS Comput. Biol.* **2012**, *8*, e1002844.
- (54) Gkeka, P.; Evangelidis, T.; Lazani, V.; Christoforidis, S.; Pavlaki, M.; Agianian, B.; Cournia, Z. Investigating the structure and dynamics of the PIK3CA Wild-Type and H1047R oncogenic mutant. *PLoS Comput. Biol.* **2014**, *10*, 10(10):e1003895.
- (55) Gabelli, S. B.; Huang, C. H.; Mandelker, D.; Schmidt-Kittler, O.; Vogelstein, B.; Amzel, L. M. Structural effects of oncogenic PI3Kalpha mutations. *Curr. Top. Microbiol. Immunol.* **2010**, *347*, 43–53.
- (56) Lovera, S.; Sutto, L.; Boubeva, R.; Scapozza, L.; Dolker, N.; Gervasio, F. L. The different flexibility of c-Src and c-Abl kinases regulates the accessibility of a druggable inactive conformation. *J. Am. Chem. Soc.* **2012**, *134*, 2496–2499.

- (57) Bono, F.; De Smet, F.; Herbert, C.; De Bock, K.; Georgiadou, M.; Fons, P.; Tjwa, M.; Alcouffe, C.; Ny, A.; et al. Inhibition of tumor angiogenesis and growth by a small-molecule multi-FGF receptor blocker with allosteric properties. *Cancer Cell* **2013**, *23*, 477–488.
- (58) Sahun-Roncero, M.; Rubio-Ruiz, B.; Saladino, G.; Conejo-Garcia, A.; Espinosa, A.; Velazquez-Campoy, A.; Gervasio, F. L.; Entrena, A.; Hurtado-Guerrero, R. The mechanism of allosteric coupling in choline kinase alpha1 revealed by the action of a rationally designed inhibitor. *Angew. Chem., Int. Ed. Engl.* **2013**, *S2*, 4582–4586.
- (59) Walker, E. H.; Pacold, M. E.; Perisic, O.; Stephens, L.; Hawkins, P. T.; Wymann, M. P.; Williams, R. L. Structural determinants of phosphoinositide 3-kinase inhibition by wortmannin, LY294002, quercetin, myricetin, and staurosporine. *Mol. Cell* **2000**, *6*, 909–919.
- (60) Panjkovich, A.; Daura, X. Exploiting protein flexibility to predict the location of allosteric sites. *BMC Bioinf.* **2012**, *13*, 273.
- (61) Segers, K.; Sperandio, O.; Sack, M.; Fischer, R.; Miteva, M.; Rosing, J.; Nicolaes, G.; Villoutreix, B. Design of protein membrane interaction inhibitors by virtual ligand screening, proof of concept with the C2 domain of factor V. *Proc. Natl. Acad. Sci. U. S. A.* **104**, 12697–12702.
- (62) Spiegel, P.; Kaiser, S.; Simon, J.; Stoddard, B. Disruption of protein-membrane binding and identification of small-molecule inhibitors of coagulation factor VIII. *Chem. Biol.* **2004**, *11*, 1413–1422.